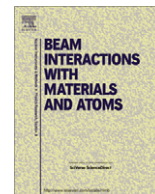


Contents lists available at [SciVerse ScienceDirect](http://www.sciencedirect.com)

## Nuclear Instruments and Methods in Physics Research B

journal homepage: [www.elsevier.com/locate/nimb](http://www.elsevier.com/locate/nimb)

## Energetics of radiation defects in Fe-based austenitic alloys: Atomic scale study

A. Bakaev<sup>a,b,d</sup>, D. Terentyev<sup>a,d</sup>, X. He<sup>c</sup>, E.E. Zhurkin<sup>d,\*</sup><sup>a</sup> SCK•CEN, Boeretang 200, Mol B2400, Belgium<sup>b</sup> Center for Molecular Modeling, Department of Physics and Astronomy, Ghent University, Technologie park 903, 9052 Zwijnaarde, Belgium<sup>c</sup> China Institute of Atomic Energy, 275-51 Xinzhen, Fangshan, Beijing 102413, China<sup>d</sup> Department of Experimental Nuclear Physics K-89, Faculty of Physics and Mechanics, St. Petersburg State Polytechnical University, 29 Polytekhnicheskaya str., 195251 St. Petersburg, Russia

## ARTICLE INFO

## Article history:

Received 13 July 2012

Received in revised form 23 December 2012

Accepted 30 December 2012

Available online xxx

## Keywords:

Radiation defects

Austenitic steels

Formation energies

Dislocation loops

## ABSTRACT

Energetics of typical radiation defects observed in austenitic stainless steel of 304L type has been characterized in the model FeNi<sub>10</sub>Cr<sub>20</sub> alloy by means of atomistic simulations employing a set of interatomic potentials specially derived to reproduce main features of 304L steel. The following defects have been considered: dislocation loops of both interstitial and vacancy nature, stacking fault tetrahedron, perfect loops and voids. The formation energy of these defects has been calculated at 0 K and the obtained results have been compared with the prediction of the elasticity theory. A good agreement has been found in all the cases except for the hexagonal Frank loop, whose sides have splitted into 1/6(112) partial dislocations, thus lowering the total formation energy. High temperature annealing, performed using molecular dynamics simulations, has proven that the considered defects are thermally stable in the temperature range 300–1200 K.

© 2013 Elsevier B.V. All rights reserved.

## 1. Introduction

Iron-based materials such as austenitic steels are important for many structural applications requiring high strength and good ductility, such as components in nuclear and fusion setups. With this respect, a good resistance against irradiation is another important requirement for such kind of materials. Neutron irradiation causes a certain degradation of the mechanical properties in these steels due to the production of radiation defects that are mainly dislocation Frank loops of self-interstitial (SIA) kind [1–3]. Free energy of lattice defects depends on its size, morphology and ambient temperature. Thus, the knowledge of the defect formation energy vs. its size allows one to predict the morphology and structure of the defects generated under neutron irradiation.

The aim of the present work is to perform atomistic numerical calculations to compute the formation energy of different radiation defects (such as SIA and vacancy Frank loops, perfect dislocation loops, stacking fault tetrahedron (SFT) and voids) with size up to 12 nm (i.e. well resolvable in transmission electron microscopy) at zero temperature ( $T = 0$  K) in the random FeNi<sub>10</sub>Cr<sub>20</sub> FCC alloy, which is used as a model for austenitic steel of 304L type. To do that, we employ a classical molecular dynamics (MD) and static (MS) simulations. The latter are performed using a set of recently developed interatomic potentials specifically derived to reproduce

main features of 304L steel [4]. A comparison of the obtained formation energy with the prediction according to the elasticity theory [5] for vacancy type defects in FCC materials is also performed. In addition, we also study thermal stability of the examined defects by means of annealing modeled using MD simulations in the temperature range 300–1200 K.

## 2. Method

We applied atomistic computer simulations in the framework of classical molecular dynamics (see e.g. [6]). The latter allows tracking individual trajectories of each atom by means of integrating Newton's equations of motion. To perform the calculations we applied a standard MD algorithm developed in [7]. The details of the defect identification are described in the same work.

To compute the interaction forces between the atoms we used a recently developed Fe–Ni–Cr potential [4], which is based on the well-known model of the embedded atom [8] and it is optimized for the correct reproduction of the mechanical properties of austenitic steels of 304L and 316L types. This potential can correctly reproduce the values of cohesive energy, lattice constants, elastic constants  $C_{11}$ ,  $C_{12}$ ,  $C_{44}$ , the energy of formation and migration of a vacancy, the formation energy of various configurations of interstitials (i.e.  $\langle 100 \rangle$ ,  $\langle 110 \rangle$  and  $\langle 111 \rangle$  dumbbells, interstitials in the octahedral and tetrahedral positions), stacking fault energy (SFE) of pure Fe, Ni, Cr and of the alloy FeNi<sub>10</sub>Cr<sub>20</sub>. In addition, a good agreement with the previously published experimental data

\* Corresponding author. Tel./fax: +7 812 552 7531.

E-mail address: [ezhurkin@phmf.spbstu.ru](mailto:ezhurkin@phmf.spbstu.ru) (E.E. Zhurkin).

**Table 1**  
Characteristics of the considered lattice defects.

| Defect type  | The size $d$ , nm | Number of point defects | Formation energy, eV/(point defect)  |
|--|-------------------|-------------------------|--------------------------------------|
| Void   | 0.7               | 17                      | 0.75                                 |
|  | 2.1               | 444                     | 0.36                                 |
|  | 3.5               | 2109                    | 0.21                                 |
| Stacking fault tetrahedron (SFT)   | 1.5               | 15                      | 0.82                                 |
|  | 3.0               | 54                      | 0.63                                 |
|  | 5.2               | 153                     | 0.50                                 |
|  | 7.0               | 276                     | 0.33                                 |
|  | 8.8               | 435                     | 0.31                                 |
|  | 10.7              | 630                     | 0.27                                 |
| Circular perfect loop $b = 1/2\langle 110 \rangle$ of interstitial/vacancy nature  | 1.4               | 36                      | 1.38 <sup>a</sup> /1.16 <sup>b</sup> |
|  | 4.2               | 316                     | 0.64 <sup>a</sup> /0.59 <sup>b</sup> |
|  | 7.0               | 887                     | 0.45 <sup>a</sup> /0.41 <sup>b</sup> |
|  | 9.8               | 1742                    | 0.37 <sup>a</sup> /0.34 <sup>b</sup> |
| Circular Frank loop $b = 1/3\langle 111 \rangle$ of interstitial/vacancy nature  | 1.4               | 31                      | 1.33 <sup>a</sup> /1.09 <sup>b</sup> |
|  | 4.2               | 253                     | 0.63 <sup>a</sup> /0.51 <sup>b</sup> |
|  | 7.0               | 733                     | 0.44 <sup>a</sup> /0.39 <sup>b</sup> |
|  | 9.8               | 1417                    | 0.35 <sup>a</sup> /0.30 <sup>b</sup> |
| Hexagonal Frank loop with the sides along $\langle 110 \rangle$ directions $b = 1/3\langle 111 \rangle$ of interstitial/vacancy nature | 1.0               | 19                      | 1.66 <sup>a</sup> /1.08 <sup>b</sup> |
|  | 3.0               | 127                     | 0.85 <sup>a</sup> /0.63 <sup>b</sup> |
|  | 5.0               | 331                     | 0.56 <sup>a</sup> /0.44 <sup>b</sup> |
|  | 7.0               | 631                     | 0.46 <sup>a</sup> /0.35 <sup>b</sup> |
|  | 9.0               | 1027                    | 0.39 <sup>a</sup> /0.30 <sup>b</sup> |
| Hexagonal Frank loop with the sides along $\langle 112 \rangle$ directions $b = 1/3\langle 111 \rangle$ of interstitial/vacancy nature | 1.7               | 43                      | 1.42 <sup>a</sup> /1.01 <sup>b</sup> |
|  | 5.2               | 343                     | 0.64 <sup>a</sup> /0.50 <sup>b</sup> |
|  | 8.6               | 931                     | 0.49 <sup>a</sup> /0.38 <sup>b</sup> |
|  | 12.1              | 1807                    | 0.45 <sup>a</sup> /0.31 <sup>b</sup> |

<sup>a</sup> Formation energy of the loop of interstitial nature.

<sup>b</sup> Formation energy of the loop of vacancy nature.

and with results obtained using *ab initio* method (the details of comparisons are given in [4]) is also achieved.

Molecular dynamics calculations were performed at  $T = 0$  K for defects of various types, whose characteristics are given in Table 1. The dimensions of the model box were  $42.4 a_0 \times 44.1 a_0 \times 53.7 a_0$  (where  $a_0$  is lattice constant equal to  $3.51595 \text{ \AA}$ ) and it contained about 400,000 atoms.

Two types of dislocation loops were considered, namely: the interstitial and the vacancy ones. Vacancy and interstitial loops were created by, respectively, the removal or introduction of atomic planes in the form of a disk taking into account the appropriate orientation of the Burgers vector and contours of the edges of extra-half plane along the dislocation line.

Then the relaxed crystals were used as initial configurations for MD calculations at nonzero temperature, whereby we investigated the stability of the defects at finite temperatures  $T$ , varied in the range 300–1200 K. The temperature was initialized by assigning velocities to each of the atoms, according to the following procedure: at the beginning the impulses of atoms are given according to the Maxwell distribution to a temperature of  $2 \times T$  (where  $T$  is the required temperature). Then we calculated the total impulse of the system, and after that we produced a simultaneous conversion of all the velocities so that the zero total impulse of the system is achieved. We used the following procedure for the establishment of dynamic equilibrium: during the first 10000 steps we

performed the integration of the equations of motion, whereas every 100 steps the moments of all atoms were renormalized so that the total kinetic energy of the system corresponded to the desired temperature.

### 3. Results and discussion

By analyzing the final configurations of the relaxed crystals containing the studied defects of interest we found that dislocation segments forming a perfect loop split in  $\{111\}$  planes into two partial dislocations (see Fig. 1a) according to the following reaction:

$$\frac{1}{2}\langle 110 \rangle \rightarrow \frac{1}{6}\langle 211 \rangle + \frac{1}{6}\langle 12\bar{1} \rangle \quad (1)$$

In the case of the hexagonal-shaped Frank loops with the sides oriented along  $\langle 110 \rangle$  directions, the sides of the loop are splitted into two partials (see Fig. 1b) by the following reaction:

$$\frac{1}{3}\langle 111 \rangle \rightarrow \frac{1}{6}\langle 110 \rangle + \frac{1}{6}\langle 112 \rangle \quad (2)$$

This splitting does not occur in the case of Frank loops with the sides oriented along  $\langle 112 \rangle$  directions (see Fig. 1c), since the dislocation segments are not contained in any of the crystallographic planes of  $\{111\}$  type.

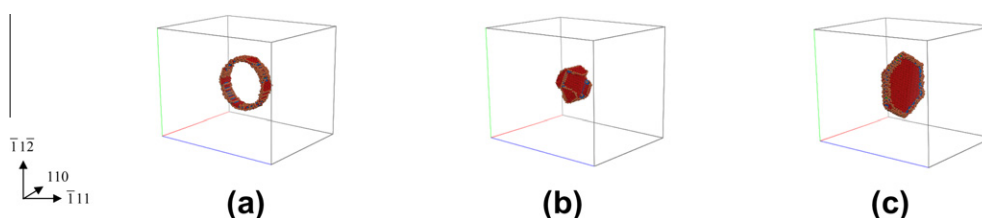


**Fig. 1.** Visualizations of final configurations of the defects: (a) interstitial circular perfect loop  $d = 9.8$  nm; (b) vacancy hexagonal Frank loop  $d = 5.0$  nm with the sides along  $\langle 110 \rangle$  directions; (c) vacancy hexagonal Frank loop  $d = 12.1$  nm with the sides along  $\langle 112 \rangle$  directions. The orientation of the crystal is the same in all figures.

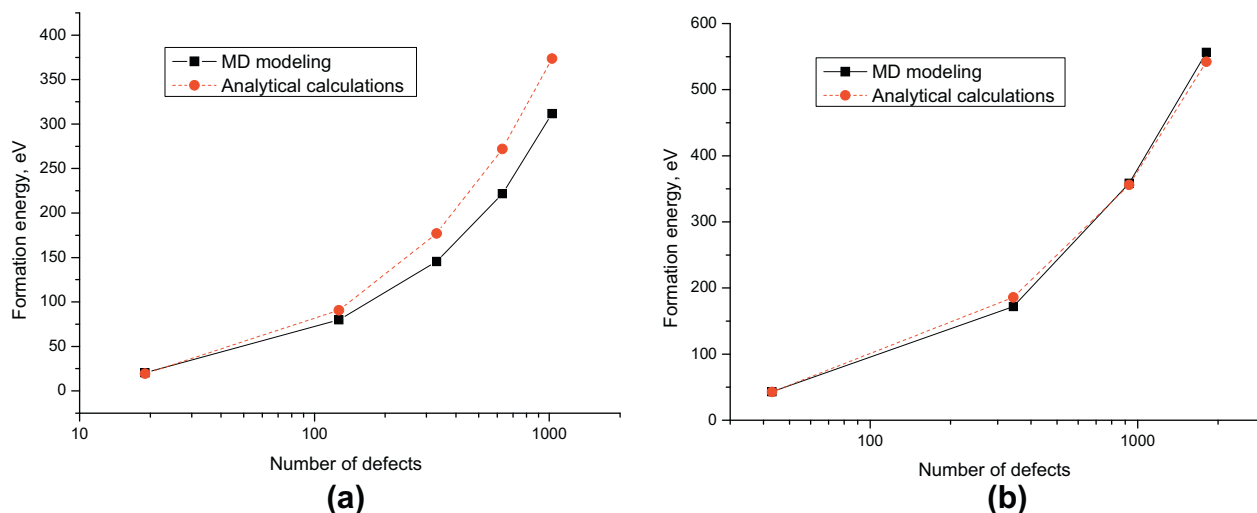


**Fig. 2.** The dependences of formation energy on the number of point defects in the configurations (a) hexagonal vacancy Frank loop with the sides oriented along  $\langle 110 \rangle$  directions; (b) hexagonal vacancy Frank loop with the sides oriented along  $\langle 112 \rangle$  directions.

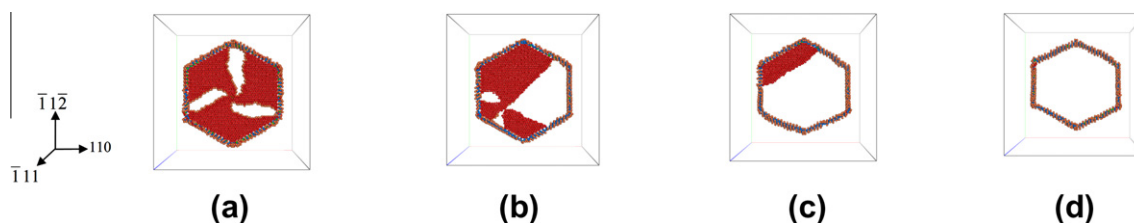


**Fig. 3.** Modeling of the interstitial Frank loop of diameter  $d = 12.1$  nm with the sides oriented along  $\langle 112 \rangle$  directions at  $T = 300$  K at the times (a) 1 ps, (b) 9 ps, (c) 12 ps and (d) 15 ps. The orientation of the crystal is the same in all figures.

The dependence of the formation energy of different defects on defect size and number of point defects (vacancies/interstitial) contained (shown in Table 1) was then analyzed. We found that in the case of interstitial-type defects in the studied range of defect sizes a hexagonal Frank loop with the sides oriented along  $\langle 110 \rangle$  directions had the lowest formation energy. Whereas in the case of vacancy-type defects, it was SFT. Note, that both types of these defects were experimentally observed (see e.g. [3]). With this regard, our results suggest that the two above-mentioned defects will be the primarily defects to be formed as a result of the evolution of displacement cascades induced by primary knocked atoms, which are in turn triggered by fast neutrons.

For the case of vacancy defects, we compared the formation energy computed using the MS calculations with the estimates obtained by analytical models, derived on the basis of elasticity theory [5,9], which is shown in Fig. 2. We found that for all types of vacancy defects the results of MS calculations well correspond to the theoretical estimates. The exception is the Frank loop with the sides oriented along  $\langle 110 \rangle$  directions (see Fig. 2a), as in this case the split of the dislocation segments lowering their self energy occurs, as mentioned above. This reaction is not accounted for in the theoretical model, which explains the observed disagreement.

Modeling of MD annealing at finite temperature for 100 ps has shown that all types of the considered defects are stable up to the highest temperature studied i.e. 1200 K. The only exception was the interstitial Frank loop with the sides oriented along  $\langle 112 \rangle$  directions. In the latter case, the transformation of the loop into the perfect one is observed to occur in a wide temperature range (300–1200 K), and this process is illustrated in Fig. 3. The latter process occurs due to the emergence (nucleation) of three pairs of partial dislocations on the loop's surface (see Fig. 3a). The nucleated dislocations repel each other and progressively eliminate the

stacking fault (see Fig. 3b and c), completely sweeping the fault (see Fig. 3d).

#### 4. Conclusions

In the considered range of defect sizes (1–10 nm), the minimal formation energy is found for the hexagonal Frank loop and SFT in the case of interstitial and vacancy types of defects, respectively. We can therefore conclude that these kinds of defects should be primary formed in austenitic steels under irradiation.

Thermal stability of the considered defects by means of MD annealing at different temperatures was also studied. All kinds of the considered defects are found to be stable in the studied temperature range except for the Frank loop with the sides oriented along  $\langle 112 \rangle$  directions. In the latter case, the transformation of Frank loop into a perfect dislocation loop was observed at 300 K and above.

For the case of vacancy defects, we compared the results of MS calculations with the estimates of analytical models, derived based on the elasticity theory [5,9]. We found that for all types of vacancy defects the results of MS calculations are in very good agreement with the theoretical estimates, except for the Frank loop with the sides oriented along  $\langle 110 \rangle$  directions, as in this case the dislocation segments split into two partials, which is not considered in the analytical treatment.

#### Acknowledgements

The author thanks FWO-Vlaanderen for their financial support. The research was partially supported by the European seventh Framework Program, under “PERFORM 60” project.

**References**

- [1] C. Pokor, Y. Brechet, J. Nucl. Mater. 326 (2004) 19.
- [2] C. Pokor, Y. Brechet, J. Nucl. Mater. 326 (2004) 30.
- [3] S.J. Zinkle, P.J. Maziasz, R.E. Stoller, J. Nucl. Mater. 206 (1993) 266.
- [4] G. Bonny, D. Terentyev, R.C. Pasianot, S. Ponce, A. Bakaev, Modell. Simul. Mater. Sci. Eng. 19 (2011) 085008.
- [5] R.A. Johnson, Philos. Mag. 16 (1967) 553.
- [6] M.P. Allen, D.J. Tildesley, Computer Simulation of Liquids, Clarendon Press, Oxford, 1987.
- [7] Y.N. Osetsky, D.J. Bacon, Modell. Simul. Mater. Sci. Eng. 11 (2003) 427.
- [8] M.S. Daw, M.I. Baskes, Phys. Rev. B 29 (1984) 6443.
- [9] J.A. Sigler, D. Kuhlmann-Wilsdorf, Phys. Status Solidi 21 (1967) 545.